ACS APPLIED MATERIALS & INTERFACES

Research Article

www.acsami.org

Photochemical Synthesis of Polymeric Fiber Coatings and Their Embedding in Matrix Material: Morphology and Nanomechanical Properties at the Fiber−Matrix Interface

Christian Kuttner,[†] Moritz Tebbe,[†] Helmut Schlaad,[‡] Ingo Burgert,[§,⊥,#] and Andreas Fery*[,†]

[†]Department of Physical Chemistry II, University of Bayreuth, Bayreuth 95440, Germany

[‡]Department of Colloid Chemistry, [§]Department of Biomaterials, Max Planck Institute of Colloids and Interfaces, Potsdam 14424, Germany

[⊥]Institute of Building Materials, ETH Zurich, Zurich 8093, Switzerland

[#]Applied Wood Research Laboratory, Empa - Swiss Federal Laboratories for Material Testing and Research, 8600 Dübendorf, Switzerland

Supporting Information

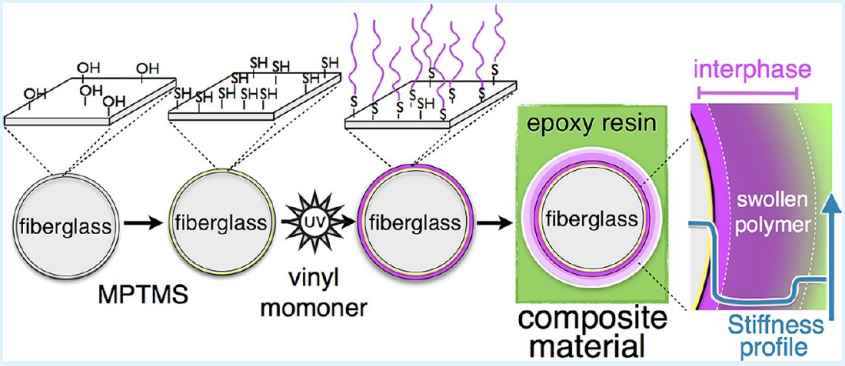

ABSTRACT: In this contribution, we present a three-step pathway to produce a novel fiber coating, study its embedding in epoxy resin and characterize its nanomechanical properties at the interface between fiber and matrix. Inorganic surfaces were sulfhydrylated for subsequent use in thiol-initiated ene photopolymerization. The influence of water on the sulfhydrylation process was studied to find conditions allowing monomolecular deposition. Surface morphology as well as SH-content were evaluated by UV/vis spectroscopy, atomic force microscopy and spectroscopic ellipsometry. Brush-like polymer layers (PS and PMMA) were introduced by UV-light initiated surface polymerization of vinyl monomers. Polymer growth and morphology were studied. After embedding, the nanomechanics of the interfacial region of the fibers was studied. AFM force spectroscopy allowed the mapping of the stiffness distribution at the cross-section of the composite with high spatial resolution. Elastic moduli were determined by Hertzian contact mechanics. The individual phases of the composite material (fiber, interphase, and matrix) can be clearly distinguished based on their mechanical response. The synthesis, morphology, and mechanical properties of an interphase based on a polymeric graft-film swollen with matrix material are shown, and perspectives of these novel coatings for improved matrix−fiber compatibility and interfacial adhesion are discussed.

KEYWORDS: *thiol−ene, polymer grafting, composite, nanomechanics, interphase, photochemistry*

1. INTRODUCTION

Fiber composites are increasingly utilized as high-performance engineering materials. They benefit from a relatively low density and good mechanical performance, which makes fiber composites favorable materials for lightweight design. Carbon fiber composites (CFC) have partly replaced metals and alloys in various applications such as airplane construction.[1] Glass fiber composites (GFC) are widely used for the production of wind turbine blades[2] or for structural elements in the automotive industry.[3]

In general, technical fiber composites are characterized by a high stiffness and strength. However, this goes along with a rather brittle fracture behavior and low impact energy absorption which still circumvents a proper utilization in various applications as it can result in catastrophic failure.[4] Interestingly, many natural composites show a surprisingly high toughness despite consisting of almost pure mineral. In glass sponges, this is achieved by a clever hierarchical structuring and by gluing mineral elements using thin soft protein layers that increase the compliance of the composite.[5] Natural fiber

Received: April 2, 2012
Accepted: June 15, 2012
Published: June 15, 2012

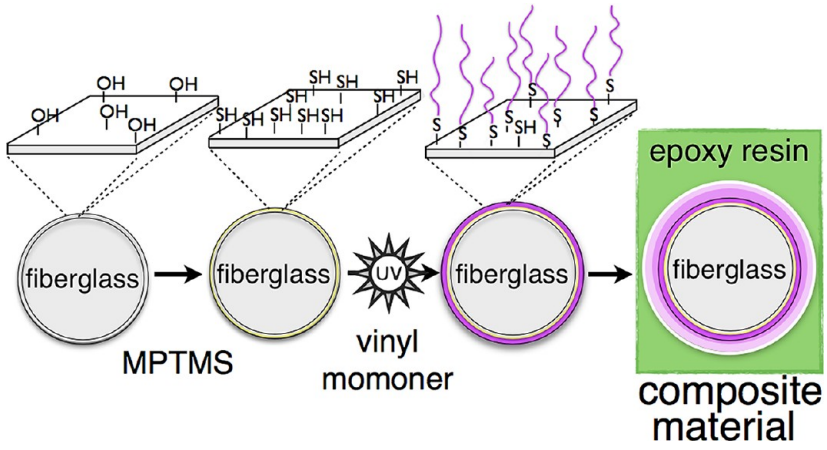

Figure 1. Three-step pathway to create a composite of polymer-grafted fiberglass in a matrix of epoxy resin: Initial sulfhydrylation introduces initiation sites followed by photochemical polymer grafting and embedding.

composites such as bone or antler achieve a high toughness by distributing compliance between different levels of hierarchy, by the design of interfaces as well as by fiber orientation patterns, which prevent crack propagation.[6−8]

Another biological concept generator for compromising between stiffness and toughness at a high performance level is the natural fiber composite of plant cell walls.[9−11] Here, stiff cellulose fibrils of a few millimeter in diameter are embedded in a soft polymer matrix.[12,13] In plant cell walls just like in mineral-protein systems, the design of the interface between the stiff phase and the soft phase is crucial for the mechanical performance of the reinforced composite.[14,15] In terms of cell walls, hemicelluloses as part of the matrix play this important mediating role.[16,17] They cover the amorphous surface of the para-crystalline cellulose fibrils and their polymer chains of different length act as coupling agents for the other matrix polymers.[18] In this way, a gradient structure is organized at the nanoscale of the cell wall, which is believed to facilitate the compliance and the toughness of the composite.

The adhesion of matrix and reinforcement of most of today's composite materials still relies mainly on (noncovalent) matchmaking.[19] The sizing of fiberglass (e.g., by increasing the surface roughness or by introduction of functional groups via silanization) are simple and cheap procedures which have become common practice in industry.[20,21] The application of sizing may enhance the composite's inner adhesion in terms of enthalpic compatibility but entropic contributions are neglected.[22,23] Natural composites have shown that optimal adhesion arises from an interplay of enthalpic and entropic contributions.[6,11,18]

In this study, we intend to transfer principles of the gradient structuring of plant cell walls to the modification of glass fiber surfaces by introducing a robust grafting method for polymers. The applied three-step pathway to produce a composite material of polymer-grafted S-2 fiberglass in epoxy resin is shown in Figure 1. Glass surfaces are first sulfhydrylated and then coated with polystyrene (PS) or poly(methyl methacrylate) (PMMA) in a photopolymerization process using UVA-light.[24,25] Polymerization proceeds in the absence of additional initiator, and the thickness of the polymer layer can be controlled by the duration of light exposure (up to ∼250 nm within 48 h). The polymer grafting process is studied in detail, and composite materials are analyzed according to nanomechanical properties.

2. EXPERIMENTAL SECTION

2.1. Materials and Reagents. Substrates: fiberglass 365 S-2 rovings, with a filament thickness of 9 μm, (AGY-Europe, France); glass slides of standard soda-lime glass (Menzel-Gläser, Thermo Scientific, Germany). For UV/vis experiments, slides of quartz glass (QSIL AG, Germany) were used; (100)-Oriented single-crystal boron-doped silicon (CrysTec, Germany). Chemicals were purchased from Sigma-Aldrich unless mentioned differently: Styrene (99.9%) and methyl methacrylate (99%) were freed from stabilizers by filtration through basic alumina column. For sulfhydrylation (3-mercaptopropyl) trimethoxysilane (MPTMS, 95%) was used. Solvents such as *n*-heptane (99%, Roth), dichloromethane (DCM, 99.8%), toluene (99.8%), unstabilized tetrahydrofuran (THF, 99.9%, Roth), and cyclohexane (99.5%) were used as received. Further reagents were 5,5′-dithiobis(2-nitrobenzoic acid) (DTNB, 99%), tris(hydroxymethyl)aminomethane (Tris, 99.9%, Roth), sodium acetate (NaAc), ammonium hydroxide (25%, Fluka), hydrogen peroxide (30%, VWR), hydrochloric acid (32%, Grüssing), 2,2′-azobis(2-methylpropionitrile) (AIBN, 98%, Fluka). Deionized water (DI) was obtained from a water purification system (Milli-Q Advantage A10, Millipore). The cold-curing epoxy resin was purchased from R&G Composite Technology GmbH, Germany: epoxy resin L (bisphenol A/F-epichlorhydrin resin) and curing agent S (Mannich base of *p-tert*-butyl-phenol and diamines). The mixture was prepared in a 10:4 ratio by mass of resin to curing agent and cured for 24 h at RT.

2.2. General Procedure of the Two-Step Polymer Grafting. Substrates were ultrasonically cleaned for 15 min in an aqueous solution of isopropanol (75 vol.%), rinsed with DI water, and immersed in a mixture of DI water, hydrogen peroxide and ammonium hydroxide (5:1:1 by volume) at 70 °C for 10 min. Activated substrates were removed from solution, and thoroughly rinsed with DI water and dried by nitrogen flow. To minimize the amount of water available for hydrolysis of MPTMS, substrates were washed with *n*-heptane before use. Direct sulfhydrylation of the activated surfaces was performed by two alternative methods: a) Fiberglass and flat substrates were immersed in a MPTMS solution of 0.1 vol.% in *n*-heptane (5.5 mM) under argon atmosphere for 12 h at RT. b) Flat substrates were placed in a dry desiccator together with a dish of 2 mL MPTMS, flushed with argon and put under vacuum for 24 h at RT. Both methods were followed by a sequential washing upon sonication (*n*-heptane, DCM, toluene, and THF for 10 min each) to remove physisorbed species. After washing, MPTMS-modified substrates were directly transferred to a 34 mol.% solution of vinyl monomer in unstabilized THF under argon atmosphere. Polymerization was carried out upon irradiation with UV−visible light (Höhnle UV F 400F, 400 W, blue filter: 320 nm < λ < 450 nm) for the respective time. The temperature was air-conditioned to stay below 30 °C. Polymer-grafted substrates were sequentially washed upon sonication (THF, DCM, toluene, cyclohexane, and DI water for 10 min each) and dried by nitrogen flow.

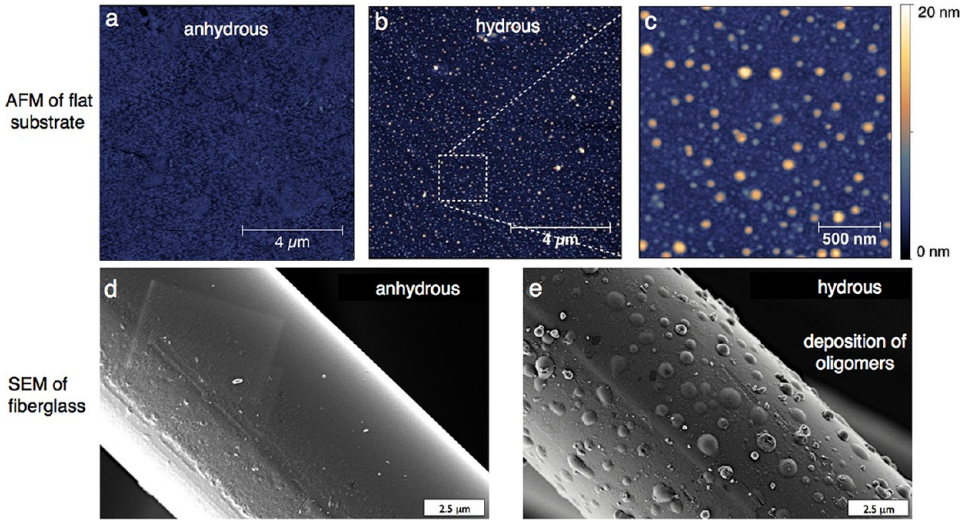

Figure 2. Micrographs of MPTMS treated surfaces: (a–c) AFM of flat substrate and (d, e) SEM of fiberglass. Anhydrous conditions allow (a, d) homogeneous deposition, whereas hydrous conditions result in (b, c, e) undesirable grainy morphologies due to deposition of agglomerated siloxane oligomers.

2.3. Surface Characterization Methods. Static contact angles of flat substrates were derived from drop shape analysis on a Dataphysics OCA20 at RT. Imaging was done by scanning electron microscopy (SEM) (Leo1530, Zeiss) and atomic force microscopy (AFM) in tapping mode (Dimension V, Veeco Metrology Group, USA) with AC160TS-W2 cantilevers (300 kHz, 42 N/m) by Olympus. Film thickness was evaluated by AFM scratch analysis and spectroscopic ellipsometry (SE) with PSCA configuration (SE850, Sentech). Dispersion data: (100)-silicon;[26] MPTMS and silicon dioxide;[27] PMMA and PS;[28] and glass.[29] The film thickness on fiberglass was calculated from thermogravimetric analysis (TGA) (nitrogen flow, heating rate of 5 °C/min, TGA/SDTA 851e, Mettler Toledo). UV/vis spectroscopy (Lambda 19, PerkinElmer) was done following Ellman et al.[30−32] with molar adsorption coefficients by Riddles et al.[33] and Eyer et al.[34]

2.4. Mechanical Characterization Methods. Nanomechanical characterization was performed on saw microtome cuts of a composite of modified fiberglass embedded in a matrix of epoxy resin, which were grinded and polished.[23] Force spectroscopy was performed with sharp tip cantilevers (NSC14, 150 kHz, MicroMash, Estonia) with typical tip radii of 10 nm on a Nanowizard by JPK AG, Germany. Cantilevers were calibrated via thermal noise[35] and cleaned in plasma (5 min, air at 0.2 mBar, 100 W; MiniFlecto, PlasmaTechnology, Germany) before use.

3. RESULTS AND DISCUSSION

3.1. Formation and Morphology of the Sulfhydrylated Surface. As a first step (see Figure 1), we introduced SH groups at model surfaces (glass substrate GS and silicon wafer SW) to allow thiol−ene photochemistry. These will function as an initiation layer upon irradiation with UV-light.[52] The goal was to create a well-defined self-assembled monolayer of MPTMS through a hydrolysis driven condensation reaction of the methoxysilyl groups with hydroxyls of the inorganic surface. Successful sulfhydrylation by MPTMS was indicated by a static contact angle of (69 ± 1)° in contrast to the activated substrates, which where fully wetted (approximately 0° for SW and <25° for GS).[36,37]

Because the formation of the siloxane layer is based on the hydrolysis of MPTMS, we investigated the influence of water on the sulfhydrylation procedure. Surface topography was evaluated by AFM, revealing a high dependency to the amount of water available for hydrolysis. Figure 2 illustrates these findings comparing anhydrous with hydrous conditions during MPTMS treatment. For anhydrous conditions dry solvents, dry instruments and inert gas atmosphere are essential (see methods 2.2). The effect of hydrous conditions (as presented in Figure 2b, c, e) was introduced by adding 0.4 vol.% aqueous HCl to the MPTMS solution to promote hydrolysis. This sensitivity is based upon the nature of the sulfhydration process. Fundamentally, the deposition mechanism discriminates two processes: termination and bridging (see Scheme 1).

Scheme 1. MPTMS Deposition Mechanism

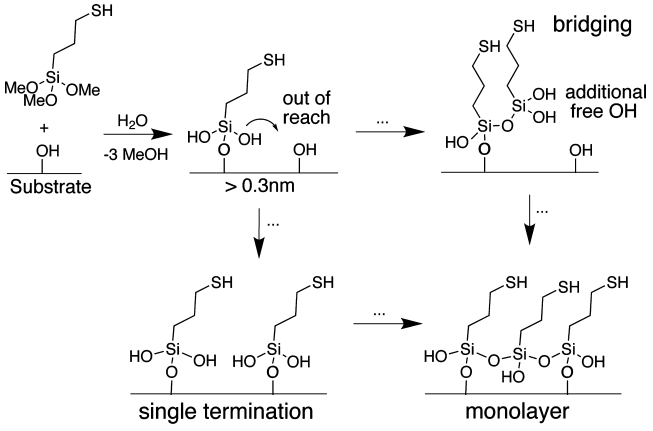

The consumption of available hydroxyls of the surface is called termination. MPTMS is hydrolyzed, if sufficient water is present in the vicinity of the surface, to its reactive siloxane species. This molecule attaches to a surface hydroxyl in terms of a single termination. Double termination, a direct attachment to two OH groups, is mostly impossible because the next surface-available hydroxyl is out of reach (approximately >0.31 nm).[38] The silanol groups of hydrolyzed MPTMS have a spacing of less than 0.27 nm. But the termination of surface hydroxyls is associated with the introduction of two new silanol groups. Consequently further molecules attach either surface terminating or as bridging species. Each bridged molecule introduces two silanol groups and, therefore, facilitates a rapid coverage of

dx.doi.org/10.1021/am300576c | ACS Appl. Mater. Interfaces 2012, 4, 3484−3492

the surface. The growth of such domains is commonly called island growth and was presented in an AFM study of OTS (*n*-octadecyltrichlorosilane) by Yang et al.[39] The balance of both deposition steps determines the resulting surface layer. To achieve monomolecular layers, bridging has to be suppressed by anhydrous conditions. A deficit of water limits the hydrolysis of MPTMS and keeps the concentration of reactive siloxanes low. If hydrolysis is possible without restraint, bridging is favored, which allows the formation of reactive solution-borne agglomerates. This may result in an undesired grainy surface structure with increased roughness and heterogeneous composition (see Figure 2). Even though this surface modification would not hinder the grafting, we regard a monolayer of sulfhydryls as the most desirable precursor layer in this context.

The theoretical thickness of an ideal monolayer of MPTMS is approximately 0.6 nm, which is hardly detectable by AFM imaging.[37,39] Therefore, spectroscopic ellipsometry (SE) on SW was used to determine the film thickness. Since MPTMS cannot be distinguished in SE, we determined the layer thickness by a difference of the apparent SiO_2 layer, before and after sulfhydylation.[26,40] Our measurements suggest the presence of a monolayer after gas-phase deposition (methods 2.2/b) with a thickness of (0.6 ± 0.1) nm. Deposition from solution (methods 2.2/a) yielded thicker layers of (1.1 ± 0.4) nm. Since the gas-phase deposition was done under inert gas atmosphere, the water content was kept at a minimum. Regarding glass substrates, SE evaluation fails due to the lack of optical contrast between siloxanes and glass. Both materials are transparent ($k = 0$) and optically isotropic ($\Delta n < 0.1$).

MPTMS deposition on fiberglass is analogous to that on flat substrates, with the amount of water available for hydrolysis strongly influencing the formation of the siloxane layer. At anhydrous conditions, which can be set by using dry solvents and temperature treatment of the fibers, the deposition is limited to thin layers with low number of aggregates (see Figure 2d). In a bundle of fibers, water easily condensates in the close gaps of adjacent fibers, which is responsible for the formation of elongated linear polysiloxane structures along the fibers. Moisture yields thicker layers with frequent accumulations of polysiloxanes (as shown in Figure 2e).

To determine the amount of free sulfhydryl on the surface, we applied a spectroscopic method developed by Ellman et al.[30] Briefly, 5,5′-dithiobis(2-nitrobenzoic acid) (DTNB) in converted to a (2-nitro-5-thiobenzoate) dianion (NTB^{2-}), which can be spectroscopically detected. Because a DTNB blind sample (SH-free) is taken as reference background, we can expect that every molecule of NTB^{2-} has been formed due to the presence of free thiols (on the sample slide). Therefore, the absorption at 412 nm is directly correlated to the amount of free thiol. Figure 3 presents the spectroscopic absorbance, which is based on a gain of NTB^{2-} and a loss of DTNB in the sample volume. The molar absorptivity of NTB^{2-} has been discussed in literature,[33,34] because it is dependent on temperature and pH of the solution. The calculated concentration of NTB^{2-} in the solution was (0.020 ± 0.001) mM. Because the number of NTB^{2-} molecules in the solution volume is equal to the number of SH functions per sample unit area, the surface concentration of thiols is (29 ± 3) SH/nm^2. Kreuzer et al. published a value of 11.1 SH/nm^2, which is in good agreement with the theoretical coverage of a monomolecular layer.[32] For a monomolecular deposition, the number of free OH groups is relevant, which for amorphous

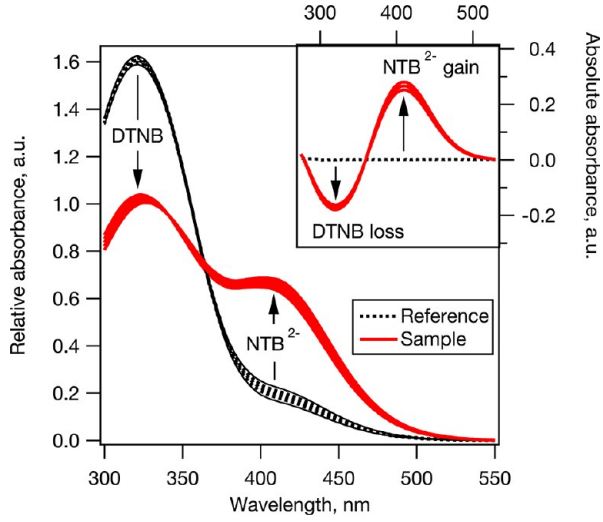

Figure 3. UV/vis-spectroscopic absorbance on MPTMS-treated sample slides. NTB^{2-} is stoichiometrically formed from DTNB by thiols. The inset shows the absolute absorbance, measured with SH-free DTNB solution as background.

silica has been examined by Zhuravlev et al.[38] Deuterio exchange combined with BET (adsorption isotherm) yielded a value of 4.9 OH/nm^2. Based on molecular dimensions and geometry, an attached siloxane molecule governs an area of 0.031 nm^2 (16% of the area available to a single surface-bound OH group). An ideal two-dimensionally polymerized lattice of siloxanes only allows 8 MPTMS molecules per nm^2. The true density is higher due to surface roughness and assembly defects. In respect to this theoretical monolayer, the measured SH content is about 3.6 times higher, suggesting a fully sulfhydrylated surface. This could be explained by the formation of nanoaggregates by bridging at the surface (see Scheme 1). This can increase the effective surface concentration of SH even in the absence of macroscopic aggregates (see Figure 2). For our proposes, this increase is favorable.

3.2. Surface Morphology of the Covalently Bound Polymer Film. We applied thiol−ene photochemistry to polymerize vinyl monomer from the sulfhydrylated surface.[41,42] Thiyl radicals are directly generated by irradiation with UV -light (>300 nm) without the help of additional photo-initiator.[52] Chain transfer reactions, especially to monomer and solvent, should be absent to avoid radical polymerization in solution and to ensure that all produced polymer chains are tethered to the surface. Note the difference to conventional free-radical surface polymerization,[37,43] where radicals are generated in solution through fragmentation of initiator molecules and transferred to the surface by hydrogen abstraction from SH. Termination via radical−radical recombination or disproportionation cannot be fully avoided but is less favorable when the concentration of radicals is kept low (→ direct generation of radicals without additional initiator) and accessibility/mobility is hindered (→ growing chains are all bound to the surface and there are no radicals in solution).

Sulfhydrylated substrates were grafted with brush-like PS or PMMA chains in THF solution by irradiation with UV-light. For PS, the success of the modification was indicated by a change of the static contact angle: PS-grafted (86 ± 1)° (in contrast to (69 ± 1)° after sulfhydrylation). The contact angle for PMMA-grafted substrates was (66 ± 2)°. Depending on the thickness of the grafted layer, a certain cloudiness can be seen

on the glass substrates. Coated silicon even appears colored due to interference effects.

An appropriate washing after the grafting procedure is of high importance. The brush-like polymer layer is swollen with unconsumed monomer, which can be washed out by good solvent upon sonication. We monitored a successive thickness decrease of the collapsed polymer layer by washing. Upon completion of the washing, the thickness in dry state stayed constant – even after swelling experiments in good solvent. The fact that the thickness (in dry state), before and after swelling, did not significantly change shows that the initial cleaning procedure did effectively remove all unbound species. The thickness of the collapsed graft layer was determined by AFM scratch analysis and SE, which were in good agreement (see Figure 4).

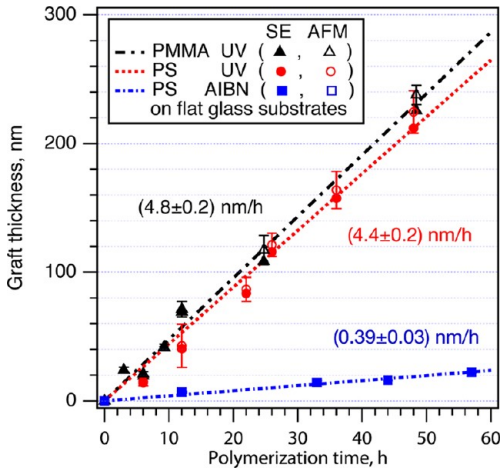

Figure 4. Linear growth of polymer layers on flat substrates. The growth rates for UV-light initiation and classical thermal initiation (by AIBN) at equal concentrations of monomer. Thickness was determined by SE and AFM scratch analysis.

Figure 4 shows the ex situ characterization of the time-dependent growth of the polymer layer in THF. Both PS and PMMA show a linear growth in a time frame of 50 h with a growth rate of about 5 nm/h. For comparison, a graft brushlike PS on sulfhydrylated surface was prepared by thermal polymerization of styrene in toluene (actually acting as chain-transfer agent) with AIBN as radical source (1:2:0.01 in mol %) at 60 °C as described by Zhao et al.[37] Growth rate of the PS layer is about 0.4 nm/h (Figure 4), which is about 1/10 of the growth rate obtained with photopolymerization. The difference in the surface grafting efficiency is attributed to the continuous generation of surface-bound thiyl radicals and absence of chain transfer and termination processes in the photochemical system.

The grafting on fiberglass proceeds analogously to flat substrates. A successful formation of a polymeric layer can be tested with electron microscopy (SEM), thermogravimetry (TGA) and spectroscopic methods (e.g., Raman). Figure 5 shows the morphology of grafted fiberglass (Figure 5b,c) in comparison to an unmodified fiber (Figure 5a). The grafted coating is clearly visible around the fiber. The thickness of the applied coating can hardly be estimated from SEM. Again SE and AFM topography are also not suited to determine the layer thickness on fiberglass. From the mass loss upon heating (TGA), the graft thickness can be calculated.

Figure 6 shows the mass loss of grafted fiberglass upon progressive heating. The polymer phase decomposes gradually, leaving only the bare fiberglass. The calculation of the coating thickness t relies on the fiber radius r, the densities ρ_i and the weight fractions w_i (of polymer p or fiberglass g) given by the mass loss.

$$t = \left(\sqrt{1 + \frac{w_p}{w_g} \frac{\rho_g}{\rho_p}} - 1 \right) r \quad (1)$$

This estimation relies on the assumption that all polymer was removed in the heating process and that the volumetric model suits the given system. The error of this estimation can be derived from Gaussian error propagation (see the Supporting Information). Density values were given by literature[44] (PMMA 1.18 g/cm^3 and PS 1.05 g/cm^3) and manufacturer (fiberglass 2.49 g/cm^3). The calculated thickness of polymer layers is in good agreement with SEM micrographs and the data from the flat substrates. The increase of layer thickness on the fiberglass is roughly linear (Figure 6b). After 12 h, the growth rates are (3.6 ± 0.1) nm/h for PS and (3.1 ± 0.1) nm/h for PMMA. These values are similar to the rates determined for flat substrates. The substrate geometry does not seem to affect the polymerization rate, as expected.

3.3. Nanomechanical Characterization. To determine the nanomechanical properties (material stiffness and elastic modulus) inside of the fiber-reinforced composite, we used AFM force spectroscopy. We probed the stiffness distribution over the fiberglass/polymer/matrix composition and evaluated the Young's modulus of the interphase region and the matrix.

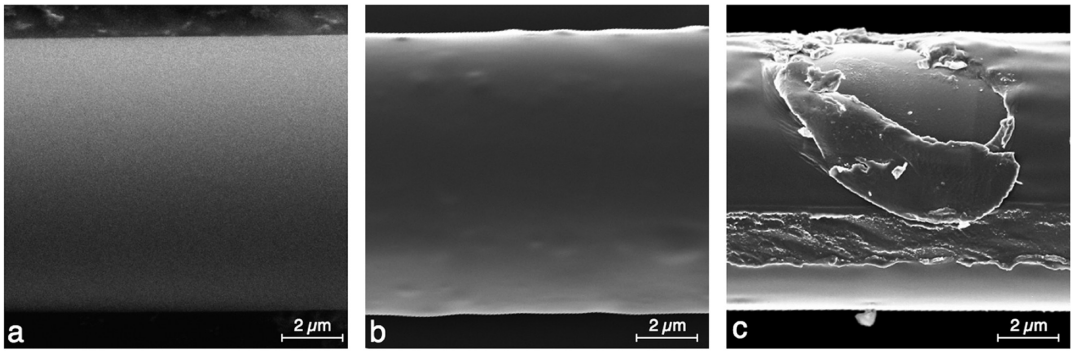

Figure 5. SEM micrographs of (a) unmodified, (b) PS-grafted, and (c) PMMA-grafted fiberglass. Image c shows a location with a defected graft-layer, which presents the sheathing of polymer around the fiber.

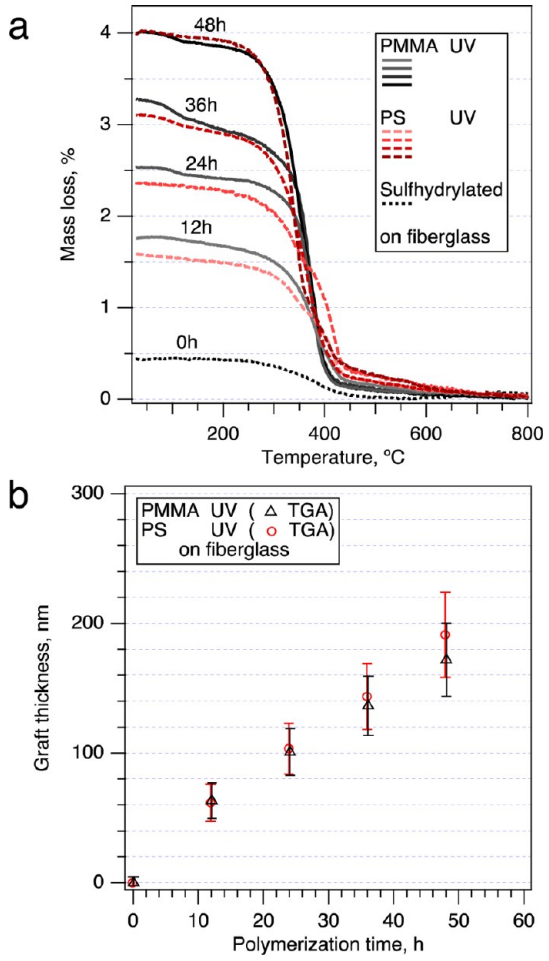

Figure 6. (a) Thermogravimetric analysis of polymer-grafted fiberglass with (b) calculated thickness estimation. After an initiation regime, the graft thickness increases linearly with time.

The polymer-coated fiberglass was embedded in epoxy resin and cold-cured for 24 h. The applied epoxy resin mainly consists of bisphenol A-epichlorhydrin (75%), bisphenol-F and 1,6-hexanediol diglycidyl ether. Curing agent is a Mannich base (40%) formed of *p-tert*-butyl-phenol, trimethylhexamethylene-diamine, and *α,α*-diamino-*m*-xylol. Upon cold curing a strong network is formed based on diglycidyl ethers of bisphenol A. Regarding the chemical composition of this network, we find phenyl groups mainly linked by ether functions. Therefore, this matrix allows the incorporation of PS or PMMA chains. Incorporated polymer chains become trapped upon curing of the network. Specimens were cut to allow access to the cross section of the formed composite material. The coating serves as a spacer, separating the two main phases of the composition and is a so-called interphase.

The cross-sections were grinded and polished to generate smooth surfaces. Fiberglass suffers brittle fraction upon mechanical strain. Perpendicular cuts are not eligible, because the points of contact between fiber stub and matrix are mechanical weak-points and already break during the cutting step. To circumvent breaking, we prepared angular cuts by cutting in a steep angle. Figure 7 presents the morphology of the prepared cross-sections. At the thick cone tip of the fiber, small grooves are formed from the matrix breaking away but leaving an intact fiber with exposed interphase. At the side of the stub, the interphase region, is intact and free of contaminations.

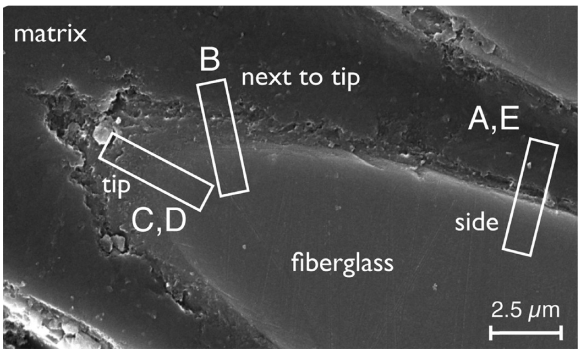

Figure 7. SEM micrograph of an angular microtome cut of grafted-fiberglass embedded in an epoxy resin matrix. Thick cone end with insets indicating location references (A–E).

The nanomechanical study was conducted by force spectroscopy with a commercial AFM equipped with a sharp tip cantilever in air. The cantilever-tip acts as a force sensor probing the surface mechanical response.[45] It is necessary to know the spring constant of the cantilever k_c in order to quantify the applied force. Its bending stiffness is determined by thermal tuning.[35,46] The quantification of the displacement is based on the precise measurement of the cantilever deflection by a position sensitive detector. For further information on AFM see reviews in literature.[47,48] Figure 8a illustrates the deformation of the surface by an AFM cantilever.

In a first step, we performed force-displacement measurements at all interfaces (see Figure 8d). In the following, we used the fiber as an undeformable reference surface in order to calibrate the system. Consequently, force-deformation data could be obtained (see Figure 8e). From the stiffness, different regimes can be recognized, which are in agreement with the height image and represent the fiberglass, an interphase region and the surrounding matrix. The stiffness of the interphase presented in Figure 8e was (20 ± 11) N/m in contrast to the matrix with (34 ± 16) N/m. For using cantilevers of different stiffness, the measured data remained in good agreement: interface (24 ± 12) N/m; matrix (35 ± 16) N/m.

To evaluate the elastic modulus from the material stiffness, we applied the Hertz model.[49,50] We used a cantilever-tip as deformation probe, with a parabolic shape. Equation 2 presents Hertz theory on the relationship of the elastic modulus E to the normal force F and the deformation δ.

$$E_{\text{surface}} = \frac{3}{4}\frac{1-\nu_{\text{surface}}^2}{\sqrt{R_{\text{tip}}}}\frac{F_{\text{Hertz}}}{\delta_{\text{surface}}^{3/2}} \qquad (2)$$

The resulting elastic moduli are in the low GPa range, which is a reasonable regime for amorphous PMMA.[51] The modulus of the matrix (4.3 ± 2.3) GPa, presented in Figure 8e, is about three times as high as the modulus of the interphase regime (1.7 ± 1.2) GPa. Table 1 summarizes the mechanical properties measured at different locations of the cross-sections (reference locations of Figure 7).

The mechanical properties determined next to the tip of the cone (B) are analogous to the data collected at the side (A, see Figure 8). At the tip of the cone (C, D), the matrix material was removed during preparation. Here, we measured elastic properties of the interphase directly along the exposed fiberglass stub. The evaluated mean Young's moduli are

dx.doi.org/10.1021/am300576c | ACS Appl. Mater. Interfaces 2012, 4, 3484–3492

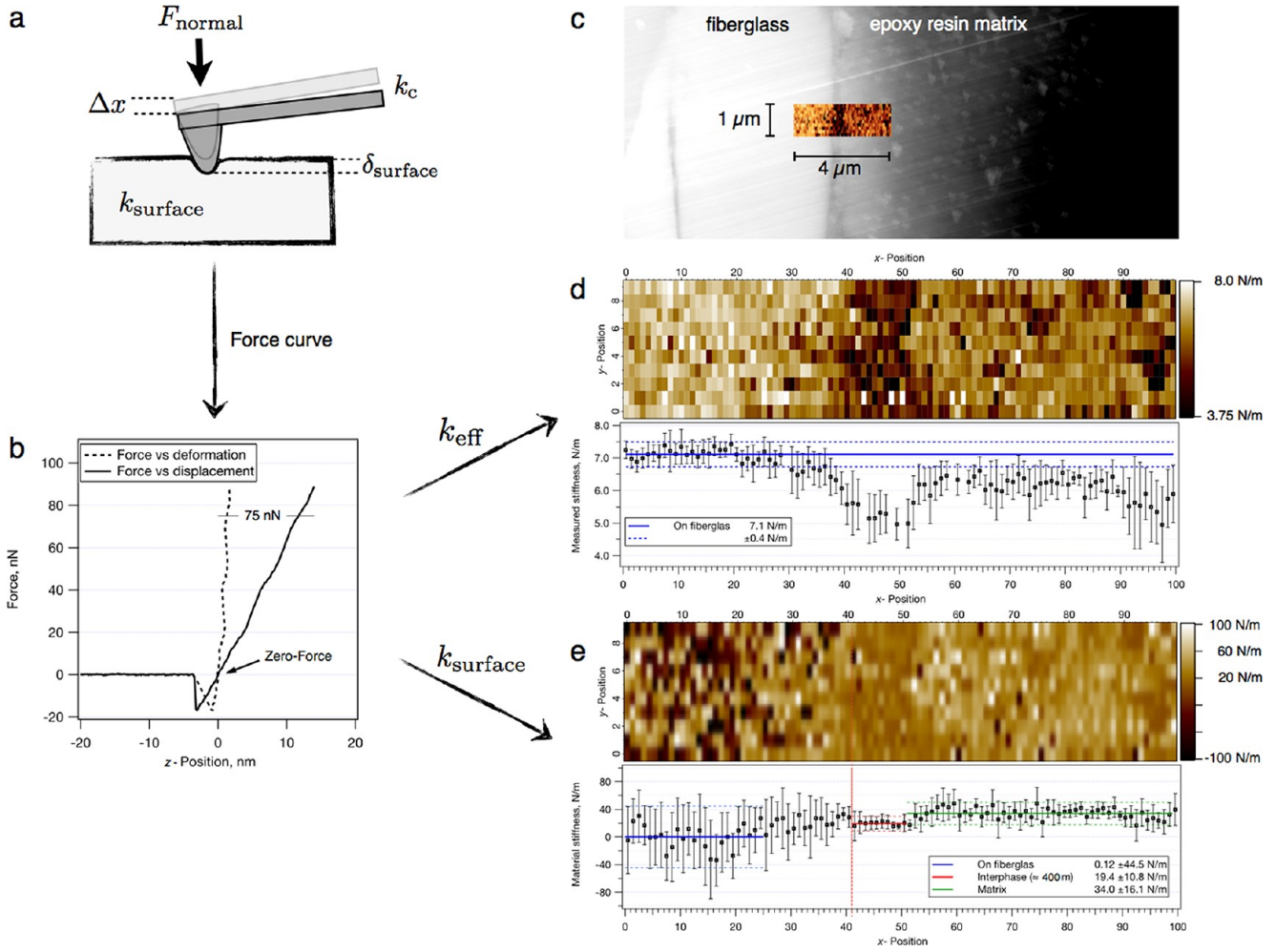

Figure 8. Mechanical properties at the interphase of the PMMA grafted-fiberglass/epoxy resin composite: (a) surface deformation schematic, (b) exemplary force curves, (c) AFM height image with overlaid force map as inset, (d) measured effective stiffness, (e) corrected material stiffness map. Maps of (d, e) are accompanied by a plot of the mean stiffness averaged over all *x*-positions.

Table 1. Mechanical Properties at the Interphase of the PMMA-Grafted Fiberglass/Epoxy Resin Composite[a]

		material stiffness (N/m)			Young's modulus (GPa)	
index	location (see Figure 7c)	cantilever, on fiberglass	interphase	matrix	interphase	matrix
A	side	7.1 ± 0.4	19.4 ± 10.8	34.0 ± 16.1	1.7 ± 1.2	4.3 ± 2.3
B	next to cone tip	7.1 ± 0.4	21.2 ± 9.1	30.0 ± 16.9	1.9 ± 1.2	4.4 ± 3.5
C	tip of cone	13.0 ± 0.8	21.2 ± 9.8		1.9 ± 1.0	
D	tip of cone	12.9 ± 0.8	27.3 ± 12.5		2.4 ± 1.4	
E	side	12.8 ± 0.8		35.0 ± 16.2		4.0 ± 2.4

[a]Index A references the example measurement presented in Figure 8. For force maps of Indices B to E, see Supporting Information.

independent from the location. E represents a location at the side, where no interphase was found. Here, the fiberglass was in direct contact to the matrix material, possibly due to a layer defect caused by preparation. In conclusion, we evaluated a mean elastic modulus of (2.0 ± 0.6) GPa for the PMMA interphase and (3.9 ± 0.6) GPa for the epoxy resin matrix.

Because the dimensions of the interphase are clearly represented in the force map (see Figure 8e) by its characteristic mean stiffness, we can estimate the thickness of the interphase layer around the fiberglass. We found a thickness of (400 ± 40) nm, which is about four times as thick as the thickness of the collapsed polymer layer (PMMA, 24 h grafting time, see Figure 6). This indicates that the PMMA brush layer has been at least partially swollen with the matrix phase – forming of a true interphase region. By comparing the thickness of the layer in embedded state with the dry state, we can clearly find that the polymer chains have incorporated into the matrix. This proofs the compatibility of polymer and resin, since the polymer graft-film would not swell in an incompatible matrix or solvent for enthalpic reasons.

4. CONCLUSION

We presented a three-step pathway to produce a composite material of polymer-grafted fiberglass in epoxy resin.

A sulfhydryl monolayer was introduced by silanization with MPTMS. Morphology, thickness, and surface concentration of

SH were characterized to have a well-defined precursor layer for further modification steps. The influence of water on the sulfhydrylation process was studied, in order to find optimal conditions. For monomolecular deposition, anhydrous conditions are essential. The surface concentration of SH corresponds to a complete coverage of the surface.

The photoinitiated grafting-from polymerization of PS and PMMA was presented on flat substrates and fiberglass. For both systems, a linear polymer growth was found after initiation. The applied thiol-initiated ene photopolymerization proved high efficiency and to be well suited to implement a polymer coating on fiberglass. By direct generation of radicals at the surface (without additional initiator) in combination with a low concentration of reactive sites, the free-radical polymerization proceeded in a controlled manner. Because polymerization in solution is avoided, growing chains are all bound to the surface, which results in a high grafting efficiency. Therewith, the thickness can be easily tailored by adaption of the polymerization time (up to ∼250 nm in 48 h). Furthermore, the applied photopolymerization shows high tolerance for functional groups, with which a broad spectrum of available vinyl monomers can be applied.

By embedding the grafted fiberglass into a matrix of epoxy resin, the polymer phase becomes partly swollen with matrix material (and increases in thickness, approximately 4 times the collapsed state). This interphase functions as a mechanical mediator between the fiberglass (>50 GPa, reinforcing phase) and the epoxy resin (∼4 GPa, ductile matrix). For force spectroscopic studies, a sharp tip cantilever was used, allowing a high spatial resolution. From the mechanical response the mechanical properties of the surface were presented in term of stiffness maps, which nicely correlate with the height images. For that reason, we were able to probe the nanomechanical properties of a PMMA-based interphase in the state of composition: stiffness of (20 ± 11) N/m; elastic modulus of (2.0 ± 0.6) GPa.

Composite materials, which are essentially multiphase materials, rely on synergetic effects by combination of materials of different mechanical properties. The chemical formulation of (polymeric) interphases can be used to adjust and control the mechanical performance of the composite as they can serve as a compatibility agent, as well as mediating mechanical gradient at the same time. Apart from simple matchmaking, the interphase can be used to control the interfacial adhesion and therewith the energy absorption capability of composites.

■ ASSOCIATED CONTENT

Supporting Information

Film thickness evaluation from AFM micrographs; Ellman method; calculation of graft thickness from TGA data; mechnical characterization; force spectroscopy data of Table 1. This material is available free of charge via the Internet at http://pubs.acs.org.

■ AUTHOR INFORMATION

Corresponding Author

*E-mail: andreas.fery@uni-bayreuth.de.

Author Contributions

The manuscript was written through contributions of all authors. All authors have given approval to the final version of the manuscript.

Funding

Financial support was given by the German Federal Ministry of Education and Research (BMBF) in the framework of a "Bionic Initiative" (0313765D).

Notes

The authors declare no competing financial interest.

■ ACKNOWLEDGMENTS

The authors appreciate fruitful discussions with Annabelle Bertin (BAM Berlin), Wolfgang Häfner (University of Bayreuth), and Georg Papastavrou (University of Bayreuth). They are also thankful to Ute Kuhn (University of Bayreuth) for the help with TGA measurements, Martina Heider (BIMF) for help with electron microscopy, and Anneliese Lang (University of Bayreuth) for help with the preparation of microtome cuts.

■ REFERENCES

(1) Soutis, C. *Plast. Rubber Compos.* **2009**, *38*, 359−366.
(2) Brondsted, P.; Lilholt, H.; Lystrup, A. *Annu. Rev. Mater. Res.* **2005**, *35*, 505−538.
(3) Corum, J.; Battiste, R.; Ruggles, M.; Ren, W. *Compos. Sci. Technol.* **2001**, *61*, 1083−1095.
(4) Sun, L.; Gibson, R. F.; Gordaninejad, F.; Suhr, J. *Compos. Sci. Technol.* **2009**, *69*, 2392−2409.
(5) Aizenberg, J.; Weaver, J.; Thanawala, M.; Sundar, V.; Morse, D.; Fratzl, P. *Science* **2005**, *309*, 275−278.
(6) Dunlop, J. W. C.; Weinkamer, R.; Fratzl, P. *Mater Today* **2011**, *14*, 70−78.
(7) Gupta, H.; Wagermaier, W.; Zickler, G.; Aroush, D.; Funari, S.; Roschger, P.; Wagner, H.; Fratzl, P. *Nano Lett.* **2005**, *5*, 2108−2111.
(8) Wagermaier, W.; Gupta, H. S.; Gourrier, A.; Burghammer, M.; Roschger, P.; Fratzl, P. *Biointerphases* **2006**, *1*, 1−5.
(9) Paris, O.; Burgert, I.; Fratzl, P. *MRS Bull.* **2010**, *35*, 219−225.
(10) Reiterer, A.; Lichtenegger, H.; Tschegg, S.; Fratzl, P. *Philos. Mag. A* **1999**, *79*, 2173−2184.
(11) Burgert, I. *Am. J. Bot.* **2006**, *93*, 1391−1401.
(12) Cosgrove, D. J. *Nat. Rev. Mol. Cell Biol.* **2005**, *6*, 850−861.
(13) Salmen, L.; Burgert, I. *Holzforschung* **2009**, *63*, 121−129.
(14) Kohler, L.; Spatz, H. *Planta* **2002**, *215*, 33−40.
(15) Fratzl, P.; Burgert, I.; Gupta, H. *Phys. Chem. Chem. Phys.* **2004**, *6*, 5575−5579.
(16) Altaner, C. M.; Jarvis, M. C. *J. Theor. Biol.* **2008**, *253*, 434−445.
(17) Keckes, J.; Burgert, I.; Fruhmann, K.; Muller, M.; Kolln, K.; Hamilton, M.; Burghammer, M.; Roth, S.; Stanzl-Tschegg, S.; Fratzl, P. *Nat. Mater.* **2003**, *2*, 810−814.
(18) Talbott, L.; Ray, P. *Plant Physiol.* **1992**, *98*, 357−368.
(19) Drown, E.; Almoussawi, H.; Drazal, L. *J. Adhes. Sci. Technol.* **1991**, *5*, 865−881.
(20) Gao, S.; Mader, E.; Zhandarov, S. *Carbon* **2004**, *42*, 515−529.
(21) Zhuang, R.-C.; Burghardt, T.; Plonka, R.; Liu, J.-W.; Maeder, E. *Express Polym. Lett.* **2010**, *4*, 798−808.
(22) Zinck, P.; Mader, E.; Gerard, J. *J. Mater. Sci.* **2001**, *36*, 5245−5252.
(23) Mader, B.; Gao, S.; Plonka, R. *Adv. Eng. Mater.* **2004**, *6*, 147−150.
(24) Hoyle, C. E.; Bowman, C. N. *Angew. Chem., Int. Ed.* **2010**, *49*, 1540−1573.
(25) Hoyle, C.; Lee, T.; Roper, T. *J. Polym. Sci. Polym. Chem.* **2004**, *42*, 5301−5338.
(26) Jellison, G.; Sales, B. *Appl. Opt.* **1991**, *30*, 4310−4315.
(27) Jellison, G.; Boatner, L.; Lowndes, D.; McKee, R.; Godbole, M. *Appl. Opt.* **1994**, *33*, 6053−6058.
(28) Kasarova, S. N.; Sultanova, N. G.; Ivanov, C. D.; Nikolov, I. D. *Opt. Mater.* **2007**, *29*, 1481−1490.
(29) Hayton, D.; Jenkins, T. *Meas. Sci. Technol.* **2004**, *15*, N17−N20.
(30) Ellman, G. *Arch. Biochem. Biophys.* **1959**, *82*, 70−77.

(31) Huffman, R. W.; Mcbride, P.; Brown, D. M. *J. Org. Chem.* **1994**, *59*, 1633−1637.
(32) Kreuzer, M.; Quidant, R.; Badenes, G.; Marco, M. *Biosens. Bioelectron.* **2006**, *21*, 1345−1349.
(33) Riddles, P.; Blakeley, R.; Zerner, B. *Method Enzymol.* **1983**, *91*, 49−60.
(34) Eyer, P.; Worek, F.; Kiderlen, D.; Sinko, G.; Stuglin, A.; Simeon-Rudolf, V.; Reiner, E. *Anal. Biochem.* **2003**, *312*, 224−227.
(35) Hutter, J.; Bechhoefer, J. *Rev. Sci. Instrum.* **1993**, *64*, 1868−1873.
(36) Bao, J.-Q.; Wang, Q.; Liu, X.; Ding, L. *Surf. Sci.* **2008**, *602*, 2250−2255.
(37) Zhao, J.; Chen, M.; An, Y.; Liu, J.; Yan, F. *Appl. Surf. Sci.* **2008**, *255*, 2295−2302.
(38) Zhuravlev, L. *Langmuir* **1987**, *3*, 316−318.
(39) Yang, S.-R.; Kolbesen, B. O. *Appl. Surf. Sci.* **2008**, *255*, 1726−1735.
(40) Malitson, I. *J. Opt. Soc. Am.* **1965**, *55*, 1205−&.
(41) Bertin, A.; Schlaad, H. *Chem. Mater.* **2009**, *21*, 5698−5700.
(42) Loebbicke, R.; Chanana, M.; Schlaad, H.; Pilz-Allen, C.; Guenter, C.; Moehwald, H.; Taubert, A. *Biomacromolecules* **2011**, *12*, 3753−3760.
(43) Forster, D.; Heuts, J.; Davis, T. *J. Polymer* **2000**, 1385.
(44) *Polymer Data Handbook*; Mark, J. E., Ed.; Oxford University Press, Oxford, U.K., 1999; p 1040.
(45) Binnig, G.; Quate, C.; Gerber, C. *Phys. Rev. Lett.* **1986**, *56*, 930−933.
(46) Hutter, J. *Langmuir* **2005**, *21*, 2630−2632.
(47) Butt, H.; Cappella, B.; Kappl, M. *Surf. Sci. Rep.* **2005**, *59*, 1−152.
(48) Tsukruk, V. V.; Singamaneni, S. *Scanning Probe Microscopy of Soft Matter: Fundamentals and Practices*, 1st ed.; Wiley-VCH: Weinheim, Germany, 2012; p 661.
(49) Hertz, H. *J. Reine Angew. Math.* **1882**, 156.
(50) Johnson, K.; Kendall, K.; Roberts, A. *Proc. R. Soc. London, Ser. A* **1971**, *324*, 301−&.
(51) Kaczmarek, H.; Galka, P. *Tribol. Lett.* **2011**, *41*, 541−554.
(52) Cramer, N.; Scott, J.; Bowman, C. *Macromolecules* **2002**, *35*, 5361−5365.